ANL/CP--76585

DE92 019041

Characterization of ^{3}He Area Sensitive Proportional Counters at IPNS for SANS Applications

RECEIVED BY OSTI

AUG 10 1992

P. Thiyagarajan, K.F. Bradley,[1] R.K. Crawford, J. E. Epperson,[2] D.G. Wozniak and J.M. Carpenter

IPNS Division, Argonne National Laboratory, Argonne, IL 60439.

[1]Department of Nuclear Engineering, Massachusetts Institute of Technology, Cambridge, MA 02139.
[2]Materials Science Division, Argonne National Laboratory.

ABSTRACT

The Small Angle Diffractometer (SAD) at the Intense Pulsed Neutron Source (IPNS) utilizes a 20 × 20 cm^2 Borkowski-Kopp type ^{3}He position sensitive detector (PSD) which has reliably performed small-angle neutron scattering experiments for more than a decade. The pulsed-source based SAD employs a small, but fixed, sample-to-detector distance and a pulsed polychromatic neutron beam. The neutron energies are resolved through time-of-flight (TOF) measurements so that a much wider range of momentum transfer is probed in a single measurement compared to the range of spectrometers using monochromatic incident beams. However, the pulsed source requires a short sample-to-detector distance so that the detector covers a large solid angle, but with lower angular resolution, and this situation puts stringent demands on the spatial resolution of the detector. Previously, nonlinearities in the position encoding of detected neutrons required that the outer channels of the detector, representing 40% of the detector area, be discarded. This paper presents a technique to characterize both the position encoding and the position resolution of the entire detector so that the whole detector can be used for SANS measurements.

2. INTRODUCTION

Small angle neutron scattering (SANS) is a general purpose technique to measure the structure and interaction of particles of 10 to 1000 Å and it has been applied to a wide range of problems in fields such as biology, polymer science, metallurgy, ceramics, micelles and microemulsions. The SANS instruments typically measure scattering in the range of momentum transfer [$q = \frac{4\pi}{\lambda}\sin(\theta)$, where 2θ is the Bragg scattering angle and λ is the wavelength of the radiation] of 0.001 to 0.3 Å^{-1}.

In the reactor-based SANS instruments, invariably, a monochromatic beam of small wavelength spread is used and the data are acquired in several steps by placing an area detector at a few sample-to-detector distances in the range of 5 to 30 m so that data can be combined to cover a wider q range. On the other hand, the SANS instruments at the pulsed-sources such as at Argonne National Laboratory,[1] at Los Alamos National Laboratory[2], at the Laboratory for High Energy Physics (KEK) in Japan[3] and at Rutherford Appleton Laboratory,[4] must use small sample-to-detector distances (due to frame overlap considerations) and use an area detector (to vary the scattering angle) and a white beam whose wavelengths can be resolved into a number of channels (to vary the wavelength simultaneously) by time-of-flight techniques. Although the technique is more complicated and laborious, this provides access to a wider dynamic q-range in a single measurement and one can take advantage of this in characterizing the disordered systems as well as in kinetic investigations.

The Small Angle Diffractometer at the Intense Pulsed Neutron Source (IPNS) has been serving as a national user facility since 1981, and has been used by scientists in a wide range of specializations.[5] This instrument sits on a pulsed neutron source in which the neutrons are produced through spallation due to the pulses (30 Hz) of 450 Mev protons impinging on an uranium target. Neutrons with wavelengths in the range of 1 to 14 Å suitable for SANS are produced by use of a 20 K decoupled liquid hydrogen moderator and a liquid nitrogen cooled MgO single

DISTRIBUTION OF THIS DOCUMENT IS UNLIMITED

crystal filter to attenuate the fast neutrons. The SAD uses a pair of crossed converging Soller collimators to provide focusing multiple aperture collimation which helps to achieve the necessary angular collimation without sacrificing flux on the sample or q resolution and while still maintaining the lowest possible q.[6] The source-to-sample and sample-to-detector distances are 7.5 m and 1.5 m respectively. An area sensitive gas proportional counter with an active volume of 20 cm × 20 cm × 3.2 cm, filled with a mixture of 65% ^{3}He and 35% CF_4 to a total pressure of 2 atmospheres, is used for SANS measurements. This detector contains an anode plane in the center, sandwiched between front and rear single wire cathode planes which produce the x and y signals.[7] The cathode wires are strung in a zig-zag pattern with 2 mm spacing, with the wire direction in the front plane being orthogonal to those in the rear. Rise-time encoding[7] utilizing a direct-time digitizer[8] produces digital x and y positions encoded with 8 bits each. Pulse height discrimination is used to eliminate events due to gamma rays and to fast neutrons, and this has been generally satisfactory.

High resolution measurement of the scattered neutron's momentum transfer vector requires accurate knowledge of both the incident and final flight paths of the scattered neutrons. The small sample-to-detector distance (covering a large solid angle and poor angular resolution) used in the pulsed-source SAD and the finite spatial resolution of the area detector puts a stringent demand on the accuracy of the detector's spatial measurement and its resolution. The Soller collimators focus the incident neutrons to a degree that the q-resolution is dominated by uncertainty in the scattered neutrons' final flight path as measured by the area detector. Furthermore a small nonlinearity in the detector, can continuously vary the channel widths along the detector and this variation can introduce systematic errors in the scattering angle determination. Since a wide range of wavelengths is employed and the data are combined in the q-space, errors in the scattering angle will corrupt the assignment of intensity in the proper q-bins. Since we are dealing with very small q-values (0.005 to 0.3 $Å^{-1}$), a small systematic error in the q values will introduce significant errors in the particle sizes determined. The parameters such as volume and molecular weight calculated from these sizes and forward scattering at $q = 0$ will be wrong due to their third power dependence on size. Samples which exhibit peaks in the scattering profiles will give erroneous periodicity in the system. Hence it becomes important to find both hardware and software solutions to improve spatial resolution and characterize and correct for the spatial nonlinearity of the area detector so that measurements can be made with higher accuracy.

The spatial resolution and the linearity of the detectors are typically counteracting. Improving one makes the other poorer. One way to reduce the nonlinearity is by altering the time constant of the preamplifier. The intrinsic RC time-constant for each cathode of SAD is ≈ 0.8 μseconds. With short amplifier time constants one can achieve better spatial resolution but this results in significant nonlinearity in the entire detector. Longer time constants produce almost linear encoding in the middle region of the detector but at the expense of spatial resolution. There are other hardware and software techniques one can use to reduce or eliminate the nonlinearities as shown by Crawford and Haumann[9] for the PSDs used for GLAD instrument which uses charge division encoding. The SAD detector electronics, however, do not have the capabilities to employ these other techniques.

To circumvent these nonlinearities up to this time, we have been using a longer amplifier time constant of 10 μseconds on IPNS-SAD to produces almost linear encoding in the central portion of the detector at the expense of reduced spatial resolution. This compromise still leaves unacceptable nonlinearities at the detector edges as seen from a flood pattern (Fig. 1) measured by using a PuBe neutron source. The finite resolution of the detector and encoding electronics smears the encoded positions so that the pattern falls to zero smoothly rather than abruptly at the edges. In addition large nonlinearities are seen at all the edge channels allowing only 60% of the area detector to be somewhat linear. It is possible to discard the data from the rest of the detector channels, but rejecting data from such a large amount of valuable detection area with nonlinearities drastically affects the range and quality of the scattering data in q-space. A much more effective solution is to measure and correct for the nonlinearity of the detector so that the higher spatial resolution and the usage of larger detector area can be achieved. Even when hardware solutions are available to fix the nonlinearity[9] software solutions to measure and correct for the nonlinearity of the detectors become handy as they can be applied to almost all the systems irrespective of the type of detectors and encoding electronics employed.

3. MATERIALS AND METHODS

A square shaped 20 × 20 cm^2 Boron nitride mask with 55 one-centimeter diameter holes distributed at regular intervals was constructed. A PuBe source was used as a neutron source. The neutrons were moderated by surrounding the source by 12 inch thick paraffin block. The area detector was placed at 1.5 meters away to obtain equal illumination throughout the detector. Flood pattern measurements were made with and without the boron nitride mask. In addition a flood pattern was also measured with a 2 mm thick cadmium sheet placed between the source and the detector to absorb the thermal neutrons. This enables one to determine the detector response for thermal neutrons by taking the difference of the two data sets.

The flood pattern measured with the mask (Fig. 2) was used to determine the peak positions and spatial resolution across the area detector by fitting with a two-dimensional Gaussian function. A typical fit using one dimensional Gaussian on a single wire is shown in Fig. 3 and the spatial resolutions (FWHM) obtained are given in Table 1. It is seen that the spatial resolution varies in the range of 6.1 to 8.2 mm (FWHM) in the central portion of the detector.

The encoded peak positions determined for the holes in the central regions where the flood pattern showed linearity and the actual positions of the holes in the mask were subjected to a two-dimensional least square fitting analysis to obtain the transformation matrix between the actual and encoded positions. Assuming a linear encoding, the inverse of the transformation matrix was used to compute recoded positions corresponding to the actual positions of the holes of the mask. Fig. 4 shows the existence of nonlinearity even in the central region of the detector and it increases as one goes toward the edges.

To correct for the nonlinearity we resorted to using the flood pattern measured with no mask (Fig. 1) to obtain the channel widths of all the individual bins. The mapped channel widths were then incorporated in the data reduction package of SAD and the agreement of the scattering from samples with known cross sections were checked. The methodology used is discussed below.

3.1 One Dimensional Case

Consider a one dimensional detector whose length R has been binned into n spatial channels with A and B indicating the edge positions so that $R = x_A - x_B$. Due to resolution effects, an event which occurs at position x' will be encoded to have been occurred at position x with probability $P(x, x')$. If we assume the resolution is Gaussian, then

$$P(x, x') = \frac{1}{\sigma(x')\sqrt{2\pi}} e^{-(x-x')^2/2\sigma^2(x')}. \tag{1}$$

If the incident intensity is $I_0(x')$, then the measured intensity pattern will be

$$I(x) = \int_{-\infty}^{+\infty} I_0(x')\epsilon(x')P(x, x')\, dx', \tag{2}$$

where $\epsilon(x')$ is the detection efficiency at position x'. This is still a continuous function in x, while the encoded intensity is actually represented in terms of the intensity in each of n channels. Let I_j be the intensity in the j_{th} channel, which spans the range from x_{j-1} to x_j. Then

$$\begin{aligned} I_j &= \int_{x_{j-1}}^{x_j} I(x)\, dx \\ &= \frac{1}{\sqrt{2\pi}} \int_{x_{j-1}}^{x_j} \int_{-\infty}^{+\infty} I_0(x') \frac{\epsilon(x')}{\sigma(x')} e^{-(x-x')^2/2\sigma^2(x')}\, dx'\, dx \end{aligned} \tag{3}$$

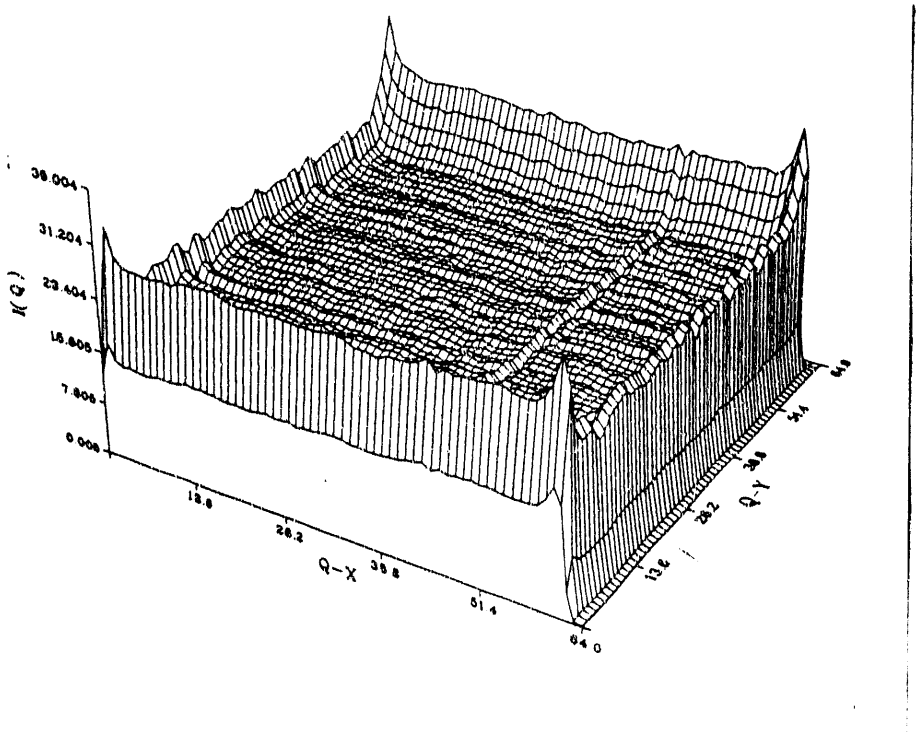

Fig. 1: Flood pattern of isotropic PuBe source measured with the SAD area position-sensitive detector.

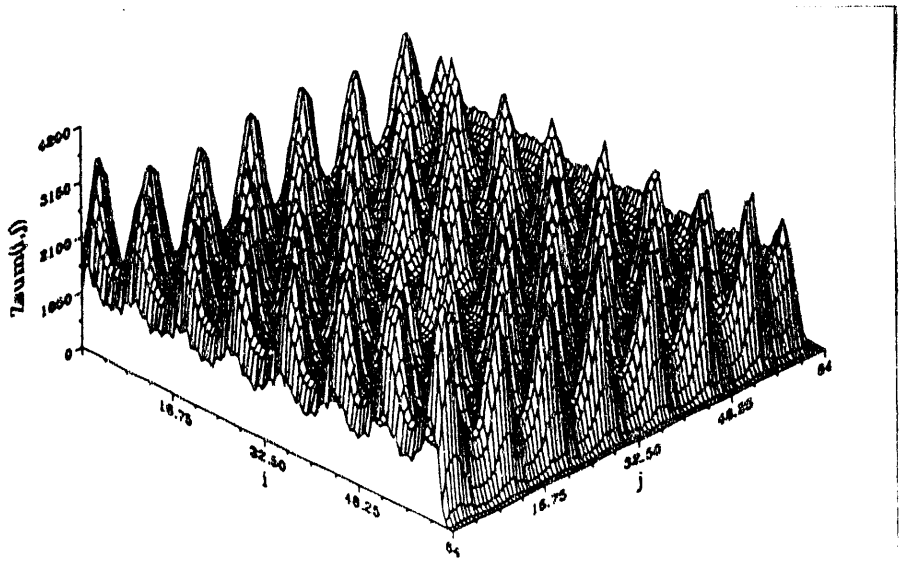

Fig. 2: Flood pattern similar to Fig. 1, but with the boron nitride mask in front of the SAD detector (see text).

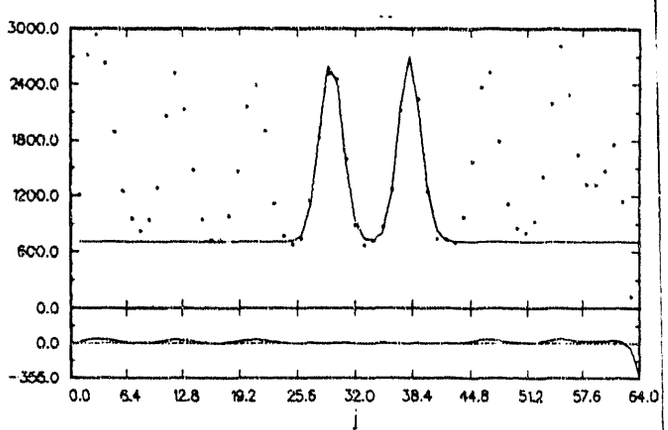

Fig. 3: One dimensional Gaussian fit of two peaks from the masked flood pattern (see Fig. 2) indicating the validity of the Gaussian resolution function.

TABLE I
Peak Positions calculated for the Mask data in the Central Region and Spatial Resolution (FWHM) from Two Dimensional Gaussian Fitting.

Spot #	Xpeak	Ypeak	sigmaX (cm)	sigmaY (cm)
1	9.807	12.359	9.060	7.852
2	18.277	12.186	8.258	7.828
3	26.875	12.035	8.008	7.501
4	35.410	11.935	7.797	7.112
5	43.983	11.882	7.353	7.827
6	52.542	11.784	7.280	7.052
7	9.863	20.904	8.123	7.551
8	18.401	20.774	8.027	7.699
9	26.943	20.616	7.828	7.744
12	52.553	20.300	7.012	7.318
13	9.937	29.455	7.642	6.805
14	18.464	29.361	8.353	7.185
15	31.326	31.093	7.383	6.619
16	44.123	29.011	7.420	7.291
17	52.642	28.888	7.279	6.985
18	10.036	38.047	8.329	6.824
19	18.521	37.948	7.746	6.628
20	27.090	37.856	7.716	6.888
21	35.643	37.766	7.728	6.866
22	44.198	37.610	7.352	6.849
23	52.736	37.542	7.001	6.909
24	10.109	46.587	8.162	6.610
25	18.585	46.498	7.955	6.944
26	27.191	46.418	8.083	6.979
27	35.718	46.327	7.961	6.777
28	44.281	46.223	7.429	6.751
29	52.790	46.122	7.172	6.760
30	10.115	55.012	7.342	6.948
31	18.684	54.971	7.525	7.074
32	27.232	54.876	8.099	7.596
33	35.793	54.753	7.431	7.024
34	44.335	54.657	7.251	7.179
35	52.883	54.552	6.111	6.870

and practical usage of eq. (3) to determine x_j from the measured I_j is given below.

3.2 Infinitely Sharp Resolution

If the resolution is infinitely sharp, the Gaussian becomes a delta function, leaving

$$I_j = \int_{x_{j-1}}^{x_j} I_0(x)\epsilon(x)\,dx. \tag{4}$$

If we make the further assumption that

$$I_0(x)\epsilon(x) = \left\{ \begin{array}{rl} 0 & \text{for} \quad x < x_A \\ I_0\epsilon(x) & \text{for} \quad x_A < x < x_B \\ 0 & \text{for} \quad x > x_B \end{array} \right\}, \tag{5}$$

then

$$I_j = \left\{ \begin{array}{rl} 0 & \text{for} \quad x_{j-1} < x_j < x_A < x_B \\ I_0\epsilon(x_j - x_A) & \text{for} \quad x_{j-1} < x_A < x_j < x_B \\ I_0\epsilon(x_j - x_{j-1}) & \text{for} \quad x_A < x_{j-1} < x_j < x_B \\ I_0\epsilon(x_B - x_{j-1}) & \text{for} \quad x_A < x_{j-1} < x_B < x_j \\ 0 & \text{for} \quad x_A < x_B < x_{j-1} < x_j \end{array} \right\}. \tag{6}$$

If two of the encoded positions are accurately known (say x_α and x_β which are at a distance L apart), then

$$LI_0\epsilon = \sum_{x_j = x_\alpha}^{x_j = x_\beta} I_j = S, \tag{7}$$

where some interpolation may be required to handle the end channels in the sum. Then

$$I_0\epsilon = \frac{S}{L} \tag{8}$$

and as long as we stay away from the ends of the pattern

$$x_j = x_{j-1} + \frac{I_j}{I_0\epsilon}, \tag{9}$$

Thus knowing any one of the x_j values we can calculate all the other values, including x_A and x_B, using eq. (9).

3.3 Broad Resolution

If the incident intensity and detector efficiency are known as in eq. (5), then eq. (3) becomes

$$I_j = \frac{I_0\epsilon}{\sqrt{2\pi}} \int_{x_{j-1}}^{x_j} \int_{x_A}^{x_B} \frac{1}{\sigma(x')} e^{-(x-x')^2/2\sigma^2(x')}\,dx'\,dx. \tag{10}$$

If we assume that $\sigma(x')$ is not rapidly varying then we can replace it with $\sigma(x)$ in this integral. Then, as long as we are several σ away from x_A or x_B, these limits can be replaced by $-\infty$ to $+\infty$, respectively. Then eq. (10) becomes

$$I_j \approx I_0\epsilon \int_{x_{j-1}}^{x_j} dx = I_0(x_j - x_{j-1})\epsilon \qquad \text{for} \quad x_A << x << x_B. \tag{11}$$

Thus the resolution effects on the flood pattern can be ignored over the central portion of the detector. In this case, two known positions x_α and x_β can again be used to determine $I_0\epsilon$ according to eqs. (7) – (8), all x_j sufficiently far from the edges can be determined from eq. (9), using one of the known positions as a starting point.

In order to determine values of x_j near x_A or x_B, we must go back to eq. (10). For example, if we need to determine x_0 through x_{n-1} near end A, we would want to use eq. (10) and the measured I_j for $j = 1$ to n, along with the value of x_n known from eq. (9) and the value of $I_0\epsilon$ known from eqs. (7) – (8) (with x_B be set equal to ∞ for this case). However, this still leaves $n+2$ unknowns (x_0 through x_{n-1}, σ, and x_A) and only n equations. The values of I_j for $j > n$ are insensitive to σ and x_A, so these additional equations are not useful.

To circumvent this, we need to measure σ in the interior portion by using a mask. If we assume that the value so determined is independent of x, then we can use this value in eq. (10) along with an assumed value for x_A to solve iteratively for each x_j, starting from x_{n-1} and working down, using these x_j values to refine the estimate of x_A and repeating the process. Alternatively, if x_A is known to be a certain distance from the starting point (say x_α), then no assumption need be made. Once we assume values for x_A and σ, then we must solve the equation

$$\begin{aligned} I_j &= I_0\epsilon \int_{x_{j-1}}^{x_j} \int_{x_A}^{\infty} \frac{1}{\sqrt{2\pi}} \sigma e^{-(x-x')^2/2\sigma^2}\, dx'\, dx \\ &= \frac{I_0\epsilon}{2}(x_j - x_{j-1}) + \frac{I_0\epsilon}{2} \int_{x_{j-1}}^{x_j} \operatorname{erf}\left(\frac{x - x_A}{\sqrt{2}\sigma}\right) dx \end{aligned} \tag{12}$$

for x_{j-1}, assuming x_j is known (since x_n is known we can start with $j = n$ and then repeat the process for smaller j values).

3.4 Two-dimensional Case

So far we have considered just a one-dimensional problem. For the SAD area detector it is a fairly good assumption that the x and y encoding is decoupled.[10,11] Hence, data for a number of y channels can be summed to provide the I_j to determine the x_j and data from x channels can be used to provide I_j to determine the y_j. Thus it is possible to map channel widths of all the 64 × 64 channels of the area detector and the mapped distances can be used to compute the scattering angles corresponding to all the spatial channels for the q determination.

4. RESULTS AND DISCUSSION

The flood patterns measured with and without the cadmium sheet were used to assess the response of the area detector for thermal neutrons. This is done by subtracting the normalized pattern corresponding to that measured with cadmium from that with no absorber. The difference flood pattern should in principle correspond to the detector response for the thermal neutrons. The flood pattern for the thermal neutrons was similar to that for all the neutrons from PuBe source but since the flood pattern corresponding to thermal neutrons was statistically poor we resorted to using that measured with no cadmium absorber in the beam.

The flood pattern corresponding to the mask was used first to determine the encoded positions corresponding to the peaks and then fitting each peak using a two-dimensional Gaussian function. The analysis of the mask-flood pattern has been used to determine the spatial uncertainty across the detector and it only varies in the range of 6.1 to 8.2 mm in the central region (table 1) and becomes larger (9 to 10.5 mm) near the edges. A linear region in the central portion of the detector has been selected for determining the channel widths in the x and y directions and the value of $I_0\epsilon$ has been determined [eqs. (7) – (8)]. We also determined the mean values for σ in the x and y directions from the same region which are 7.6 and 7.4 mm (FWHM) in the x and y directions respectively. In all the calculations these σ values were used for determining the positions. The mapping of the channel widths in the outer regions was

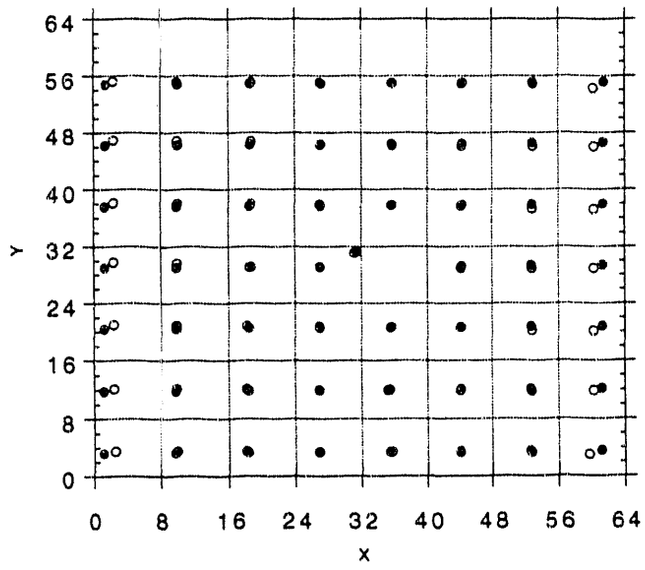

Fig. 4: Open circles indicate the channel number of the centroids of the peaks measured in the masked flood pattern. Filled circles are the expected peak positions given the mask hole positions and assuming linear position encoding.

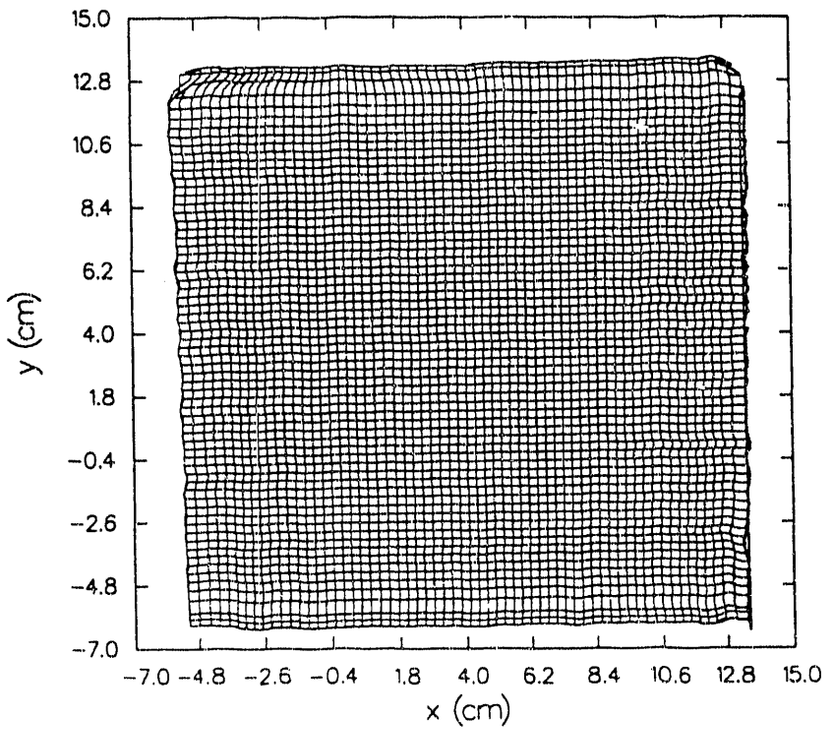

Fig. 5: The detector spatial-bin boundaries determined from the flood pattern as described in the text.

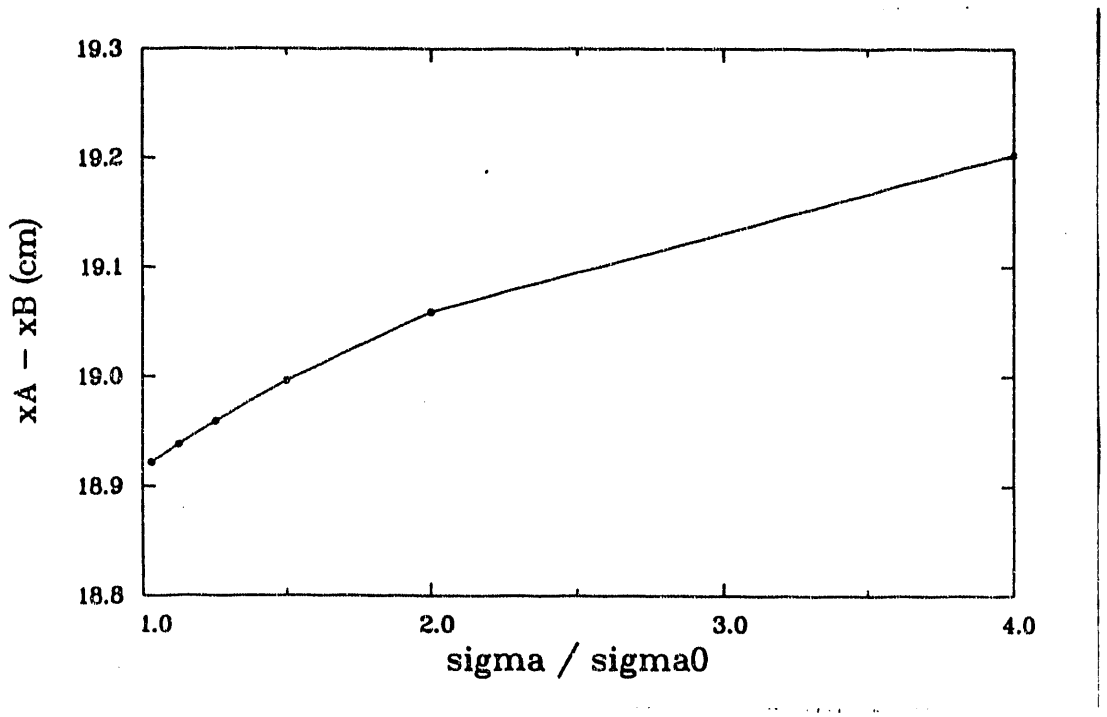

Fig. 6: The dependence of the apparent detector active area as a function of the detector resolution.

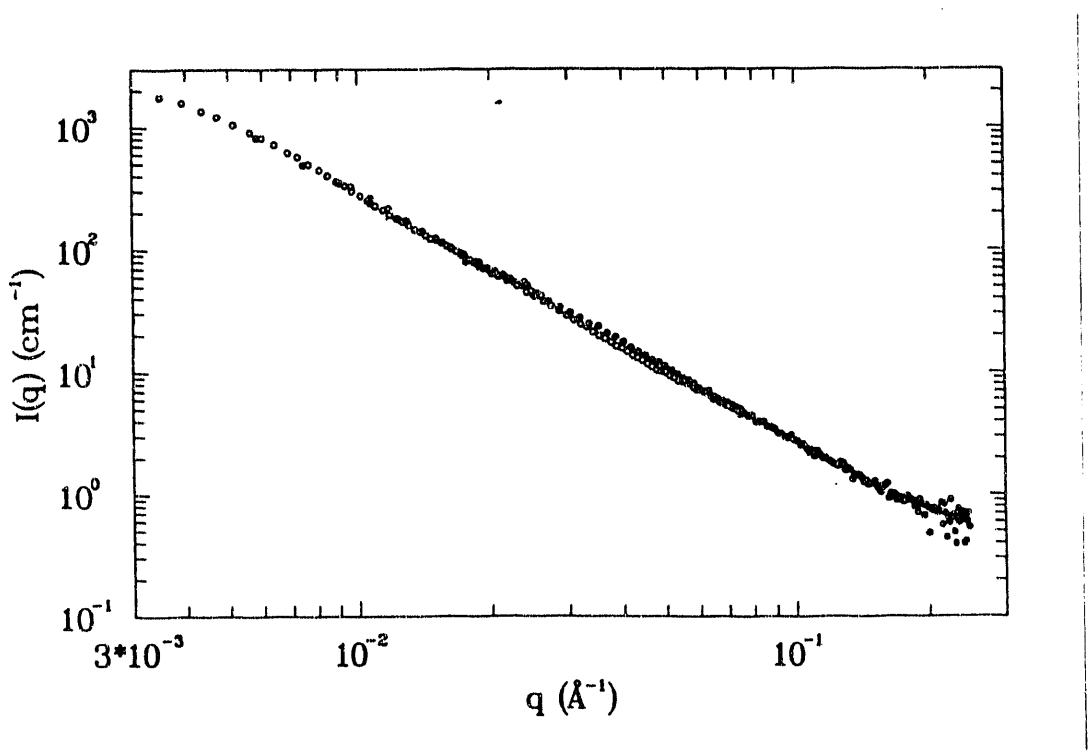

Fig. 7: The differential scattering cross section of the polymer sample as measured at ORNL (open circles) and at SAD corrected for the detector nonlinearities (filled circles).

done by using eq. (12) and the mapped channel widths are shown in Fig. 5. As expected, the channel widths are increasing as one goes from the central region to the edges.

4.1 Effect of Detector Resolution:

Although the measured resolution falls in the range of 6.1 to 8.2 mm FWHM in the central region, it becomes larger at the edges. It is also difficult to measure accurately using a mask as the peaks are not well defined at the edges due to large nonlinear effects. Hence we varied the detector resolution from 6 to 12 mm (FWHM) and mapped the channel widths. As expected the channel widths in the central portion were not affected by this. However the channel widths in the edge channels tend to increase with the increase in the uncertainty. The total widths of the detector in the x and y directions increase only by 0.2 to 0.3 cm as the σ values in the central regions are doubled (Fig. 6).

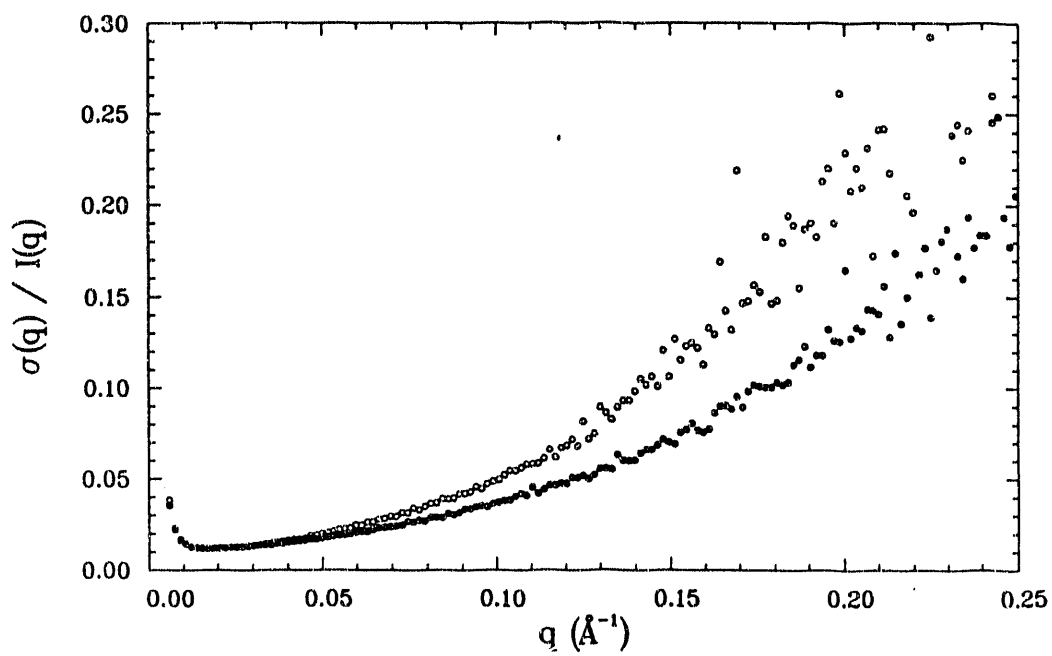

Fig. 8: The ratio of the standard deviation of each point in Fig. 7 to the the intensity values as a function of q. Open circles show this ratio when useful detector area is limited by edge effects. Filled circles show the same result when the nonlinear corrections allow use of the full detector area.

4.2 Scattering Measurements

We have chosen two samples to test the correctness of the positions calculated using the above technique. These samples are a polymer and a silica gel powder that have been measured at the SANS instruments at High Flux Reactor at ORNL and D11 at the ILL in France as well as at IPNS-SAD. In order to test the very low q region the data from the silica gel was used. A Guinier analysis [$\ln(I(q))$ vs. q^2] of the data from ORNL gave a Guinier Rg of 44.9 $\pm$ 0.5 Å. The data from D11 also gave similar results. Analysis of the data from SAD gave excellent agreement with an Rg of 45.0 $\pm$ 0.7 Å after the correction for the nonlinearity was made. The data from the central portion obtained through linear encoding gave an Rg of 44.8 $\pm$0.9 Å. Thus in the case of linear encoding the statistical accuracy of the particle sizes determined in the low q region is affected by the utilization of the smaller detector area.

To test the quality of the data in the whole q region accessible to SAD instrument we have used a polymer sample. This sample has a 50:50 ratio by weight of hydrogeneous and perdeuterated high molecular weight polystyrene and exhibits a q^{-2} dependence of scattering intensity . The data for this sample from ORNL and also that from SAD corrected using the above technique are shown in Fig. 7. It is clearly seen that the SAD data agrees well with that from ORNL in the low-q region and the SAD data extends to much larger q domain. These results support the validity of the technique used for the determination of accurate positional information for the area PSD at SAD.

The correction for nonlinearity of the detector permits access to using a larger area of the two dimensional PSD. This in turn improves the statistical precision of the data in the whole q range. The area PSD at SAD has acceptable linearity only in the central portion which spans only 60% of the detector's area. We have processed the data from SAD for the polymer sample with both linear encoding (using the central 60% of the detector area) and nonlinear encoding of the positions using the whole detector. The ratio of $\sigma(q)/I(q)$, where $\sigma(q)$ is the standard deviation in the $I(q)$ value, is plotted as a function of q for both cases in Fig. 8. In both cases the $\sigma(q)$ has similar values up to $q = 0.035$ Å^{-1}, but, as expected, it becomes larger for the linear binning case with increasing q. In addition, the $\sigma(q)$ values become more scattered in the high-q region for the linear encoding case compared to the nonlinear encoding.

5. CONCLUSION

The linear and area detector PSDs essential for the measurement of scattered neutrons have variations in detector sensitivity, spatial resolution and channel widths across the detector, irrespective of the type of detector and encoding electronics used. The correction for the detector sensitivity variation is easily done by normalizing for the counts in each pixel while performing the data reduction. However, the variation of the channel widths, due to differential encoding nonlinearities across these detectors cause significant errors in the results obtained from experiments such as SANS. Improving the linearity at the expense of spatial resolution can be made by tuning the electronics. SANS instruments at pulsed sources require higher spatial resolutions than can be obtained by this tuning. Substantial nonlinearities still exist at the detectors' edges making the measurement and correction of these nonlinearities essential in order to use the largest possible detector area. This effort yields reduced uncertainty in measured intensity across the spectrometer's entire q-range as well as making more precise position measurements possible. It is hoped that this second improvement will allow a substantial increase in future measurements' q-resolution because of the much finer detector binning that is now possible.

6. ACKNOWLEDGMENTS

This work benefited from the use of the Intense Pulsed Neutron Source which is funded by the Unites States Department of Energy, Office of Basic Energy Sciences and other Department of Energy Programs under contract W-31-109-ENG-38 to the University of Chicago. The authors also thank Professor Frank S. Bates (University of Minnesota) for providing the polymer sample. In addition, we are grateful to Dr. Rex Hjelm (LANL), Dr. George Wignall and Dr. Stephen Henderson (ORNL), and Dr. Peter Lindner (ILL) for assisting in the measurements reported here and many fruitful discussions.

7. REFERENCES

[1] J.E. Epperson, J.M. Carpenter, R.K. Crawford, P. Thiyagarajan, T.E. Klippert and D. G. Wozniak "The Time-of-Flight Small Angle Diffractometer At The Argonne Pulsed Neutron Source," *J. Appl. Cryst.*, to be submitted.

[2] P.A. Seeger, R.P. Hjelm and M.J. Nutter, "The Low-q Diffractometer At The Los Alamos Neutron Scattering Center," *Mol. Cryst. Liq. Cryst.*, **18A**, 101-117 (1990).

[3] Y. Ishikawa, M. Furusaka, N. Niimura, M. Arai and K. Hasegawa, "The Time-of-Flight Small-Angle Scattering

Spectrometer SAN At The KENS Pulsed Cold Neutron Source," *J. App. Cryst.*, **19**, 229-242 (1986).

[4] R.K. Heenan, R. Osborn, H.B. Stanley, S.M. King, D. F. R. Mildner and M. Furusaka, *J. App. Cryst.*, 1992 (to be submitted).

[5] J.E. Epperson, P. Thiyagarajan, J.M. Carpenter, R.K. Crawford and D.G. Wozniak, "Small Angle Neutron Scattering with the SAD at IPNS," *IPNS 1991 Progress Report*, ed. F.J. Rotella (1991).

[6] R.K. Crawford, J.E. Epperson and P. Thiyagarajan, "Soller Collimators for Small-Angle Neutron Scattering," ICANS, 1988.

[7] C.J. Borkowski and M.K. Kopp, "Design and Properties of Position-sensitive Proportional Counters Using Resistance-capacitance Position Encoding," *Rev. Sci. Instr.*, **46**, 951-962 (1975).

[8] F.J. Lynch, "Direct Position and Time Digitizer for Position-sensitive Proportional Counters," *IEEE Trans. Nucl. Sci.*, **NS-27**, 327-328 (1980).

[9] R.K. Crawford and J.R. Haumann, "Nonlinearities In The Charge-Division Encoding Of Position-sensitive Detectors," *Nuc Inst. and Methods in Phys. Res.*, **A292**, 657-670 (1990).

[10] C.J. Borkowski and M.K. Kopp, "Some Applications and Properties of One- and Two-dimensional Position-Sensitive Proportional Counters," *IEEE Trans. Nucl. Sci.*, **NS-17**, (3), 340-349 (1970).

[11] C.J. Borkowski and M.K. Kopp, "Proportional Counters Photon Camera," *IEEE Trans. Nucl. Sci.*, **NS-19**, (3), 161-168 (1972).

DISCLAIMER

This report was prepared as an account of work sponsored by an agency of the United States Government. Neither the United States Government nor any agency thereof, nor any of their employees, makes any warranty, express or implied, or assumes any legal liability or responsibility for the accuracy, completeness, or usefulness of any information, apparatus, product, or process disclosed. or represents that its use would not infringe privately owned rights. Reference herein to any specific commercial product, process, or service by trade name, trademark, manufacturer, or otherwise does not necessarily constitute or imply its endorsement, recommendation, or favoring by the United States Government or any agency thereof. The views and opinions of authors expressed herein do not necessarily state or reflect those of the United States Government or any agency thereof.

The submitted manuscript has been authored by a contractor of the U. S. Government under contract No. W-31-109-ENG-38. Accordingly, the U. S. Government retains a nonexclusive, royalty-free license to publish or reproduce the published form of this contribution, or allow others to do so, for U. S. Government purposes.

END

DATE
FILMED
9/23/92